Collapse of submerged granular columns in loose packing: experiment and two-phase flow simulation

Cheng-Hsien Lee,¹ Zhenhua Huang,^{2, a)} and Ming-Lan Yu³

- ¹⁾ Department of Water Resources and Environmental Engineering, Tamkang University, Taiwan
- ²⁾Department of Ocean and Resources Engineering, School of Ocean and Earth Science and Technology, University of Hawaii at Manoa, Honolulu, Hawaii 96822 USA
- ³⁾Department of Civil and Coastal Engineering, University of Florida, Gainesville, Florida 32611, USA

(Dated: Wednesday 6th March, 2019)

This study examines, both experimentally and numerically, the collapse process of a submerged granular column in loose packing, with an emphasis on the effects of the grain size and the initial aspect ratio of the granular column. A two-phase flow continuum model, developed based on the rheological characteristics of solid-water mixtures, is used to perform the numerical simulations. Two particle sizes representing very fine particles and coarse particles are examined in this study. The two-phase flow model is validated and verified by comparing with the measured characteristics of the collapse process. Compared to the collapse of a granular column of coarse particles, the runout distance of a granular column with very fine particles is longer and the spread velocity is higher. Based on the two-phase flow simulation results supported by the experimental results, critical initial aspect ratios are identified to classify the types of the initial collapse process and the final deposit morphology, and the empirical expressions are provided to describe the changes of the runout distance, collapse duration, final deposition height, and spread velocity with the initial aspect ratio. A phenomenon similar to the so-called Kelvin-Helmholtz instability can be observed in both the experiment and the simulation at the later stage of the collapse, which causes the formation of several vortexes in the two-phase flow during the collapse process. The presence of these vortexes is responsible for the pressure drop on the bed after the passage of the flow front and the wavy feature on the final deposit morphology.

a) Author to whom correspondence should be addressed. Electronic email: zhenhua@hawaii.edu

I. INTRODUCTION

Submarine granular flows consist of a mixture of water and solid particles, where the interfacial forces such as drag play important roles in determining the flow behaviors. When the volumetric concentration of the particles is high, the inter-particle collisional and frictional force also affect the flow behaviors considerably¹. In order to understand the rheological characteristics of submerged granular flows, some studies in the literature focused on the submerged granular flows on inclined planes²; these studies have found that the concentration and the effective friction depend on either the inertial number (the ratio of the particle inertial force to the confining pressure) or the viscous number (the ratio of the viscous stress to the confining pressure). Another class of problems studied in previous studies is the collapse of submerged granular columns^{3–5}, which have also been used as idealized models to understand submarine landslides. In most of experimental studies concerning the collapses of granular columns (dry or submerged), a two-dimensional (2D) geometry is usually employed where the granular columns are initially confined by two vertical walls^{3–7}; after the front wall is suddenly removed, the granular material collapses.

When the surrounding fluid has a much lower density than the solid grains (e.g. the solid particles are glass beads and the fluid is air), the effects of the fluid on the collapse process can be safely ignored. In such a situation, the kinematic features and deposit morphology depend mainly on the aspect ratio of the two-dimensional granular column in consideration⁶: the normalized runout distance is a power-law function of the aspect ratio $A = H_i/L_i$, where H_i is the initial height and L_i is the initial length; the deposit morphology is triangular-shaped when $A \geq 0.7$ and trapezoid-shaped when $A \leq 0.7$; and the duration of the collapse process, t_d , is proportional to the square root of the initial height of the column⁶. Other parameters such as particle diameter, d, have insignificant effects on the collapsing processes⁷ if the surrounding fluid has a much lower density than the solid particle.

When the surrounding fluid has a density comparable to that of the solid particles (e.g., the solid particles are glass beads and the fluid is water), the effects of the fluid on the collapse process are significant. The spreading speed of the flow front for a granular column submerged in water, u_f , is slower than that for the same granular column in air^4 , and increases with Archimedes number, $Ar = g'd^3/\nu_f^2$, where ν_f is the kinematic viscosity of the fluid and $g' = g(\rho_s - \rho_f)/\rho_f$ is the effective acceleration due to gravity with ρ_s (or ρ_f) being

the density of particle (or fluid). Physically, Archimedes number is the ratio of the external force to the internal viscous force and it measures the momentum transfer by the drag between the fluid and the solid particles. Based on their two-dimensional DEM (Discrete Element Method) simulations, Topin et~al.⁸ found that the runout distance of a granular column submerged in water could be either below or equal to that of the same granular column in air. This is attributed to the compensation between the fluid viscous effect and the lubrication effect: during the collapse of a submerged granular column, the viscous effect reduces the kinetic energy of the solid particles but the lubrication effect enhances the flow of the granular material. For granular columns submerged in a high viscous fluid, Rondon, Pouliquen, and Aussillous⁵ found experimentally that the initial concentration, c_i , could affects the collapsing process significantly: a granular column with an initially loose packing has a faster collapse process and a longer runout distance compared to the same granular column but with an initially dense packing . Wang et~al.⁹ used water in their experiment and observed the same phenomenon.

It has been hypothesized that: for initially loose packing, the contractancy of the granular column at the initial stage of collapse may squeeze fluid out of the column, which helps to destabilize the granular column; for the initially dense packing, however, the dilatancy of the granular column at the initial stage could absorb the fluid into the column, which helps to stabilize the column⁵. Recently, Santomaso, Volpato, and Gabrieli ¹⁰ experimentally studied the collapse of wet granular columns.

There are several numerical studies in the literature on the collapse of submarine granular columns. Savage, Babaei, and Dabros ¹¹ proposed a single-phase mixture model to study the collapse of a submerged granular column, where the Coulomb friction was adopted to compute the inter-particle friction force. However, single-phase mixture models are not able to consider the fluid-particle interaction satisfactorily. Meruane, Tamburrino, and Roche ⁴ first developed a two-phase model to simulate the collapse of a submerged granular column. A similar two-phase model was recently developed by Si, Shi, and Yu ¹². Meruane, Tamburrino, and Roche ¹³ extended their model ⁴ to deal with granular flows of binary mixtures of solid particles; their two-phase model considered the fluid-particle interaction by including terms accounting for the drag force between the two phases in the momentum balance equations. However, Meruane, Tamburrino, and Roche ⁴ used a combination of Coulomb friction and the kinetic theory to develop their constitutive model for the solid-phase stress, which

may not be suitable for high concentration flows with fine particles. When solid particles are immersed in a fluid, the particle size also affects the interaction between the fluid and the solid particles, and thus the rheological characteristics². Lee, Low, and Chiew¹⁴ developed a two-phase model for sediment transport, which adopted the rheological characteristics for both coarse and fine particles. The model of Lee, Low, and Chiew¹⁴ was later extended to study the collapse of a granular columns submerged in a fluid under initial loose packing or dense packing¹⁵.

Different from a previous study of Lee and Huang 15 , in which the emphasis was on the effects of initial packing conditions, this study emphasizes on the effects of particle size and aspect ratio. We use glass beads of the same density as the solids particles and the water as the fluid. To examine possible effects of particle size, we consider two particle diameters: d = 0.12 mm (very fine particles in the Wentworth scale) and 0.56 mm (coarse particles). We use the two-phase model developed by Lee and Huang 15 to perform the numerical simulations. After the validation of the two-phase model by comparing the numerical simulated and observed collapse processes, we present the computed flow and pressure fields and use them to explain some phenomena observed in the experiment and understand some important physics involved in the collapse process.

II. EXPERIMENTAL SETUP

Fig. 1 shows a sketch of the experimental set up. The experiment was performed in a glass water tank, which was 120-cm long, 20-cm wide and 30-cm high. A false bottom made of a Perspex plate was placed on the bottom of the tank, and the height of the false bottom was 9 cm. The reason to have a false bottom is to avoid the field of view being blocked by the lower frame of the tank. A layer of glass beads with diameter d = 0.506 mm was glued onto the surface of the false bottom. Two vertical Perspex walls were positioned on the left end of the tank to create a reservoir for the granular material (glass beads). The left wall of the reservoir had an L-shape and was fixed firmly onto the false bottom using an F-clip, and the right wall of the reservoir was designed as a mobile gate which can be lifted up at a high speed. To achieve this, the gate was connected to a sliding rail system. To avoid vibration when the gate was moving, two perspex plates with the same thickness of 5 mm were fixed to the side walls with a gap in between so that the gate can slide in the gap

smoothly. Glass beads (Potters Cooperation) were used as the solid particles, and the liquid was the tap water with $\rho_f = 1000 \text{ kg/m}^3$ and $\nu_f = 10^{-6} \text{ m}^2/\text{s}$ at the room temperature. The properties of the glass beads are listed in Table I: according to the Wentworth scale, Particle AE belongs to very fine particles and Particle B belongs to coarse particles. A high-speed camera (Fastec-IL5) was used to record the collapse processes at a frame rate of 400 frames per second and with a resolution of 2560 x 1000 pixels.

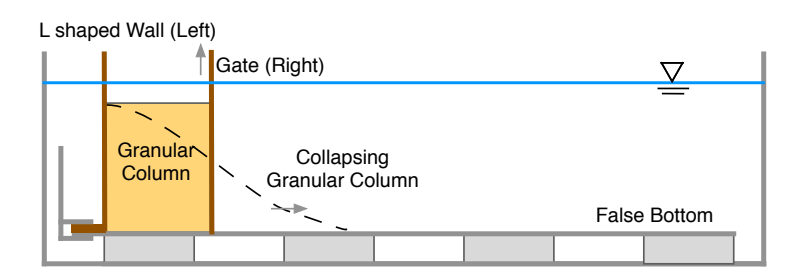


FIG. 1: Schematic diagram of experimental set up.

In the experiment, the length of the granular column (the dimension along the longitudinal direction of the tank) was fixed at 3.0, 6.0 or 9.0 cm, and the height of the granular column varied from 1.5 cm to 11.0 cm for each column length. The width of the column was the same as the width of the tank, which was 20 cm. The aspect ratio ranged from 0.2 to 4.0. The experimental procedure is outlined as follows: (i) the tank was filled with the water to a designed depth; (ii) the glass beads were poured into the reservoir; (iii) the water depth above the false bottom was adjusted to 15 cm by adding or removing water; (iv) a whisk driven by a drill motor (both are off-the-shelf products) was used to suspend the particles in the reservoir; (v) after all the particles had settled down in the reservoir, the gate was removed rapidly by hand to initiate the collapse of the granular column.

Based on the measurement procedure description in Appendix A, the granular column in the experiment had an initial volume concentration $c_i \approx 0.55$ with a 0.7% error for both particle sizes. The initial solid friction of 0.55 was also used by Rondon, Pouliquen, and Aussillous⁵.

If the particles do not go through the suspension-deposition process, $c_i \approx 0.6$. According to Rondon, Pouliquen, and Aussillous⁵, $c_i \approx 0.55$ corresponds to a loose packing and $c_i \approx 0.6$ corresponds to a dense packing. Previous studies have found that the initial packing has significant influence on the collapse process⁵. This study concerns only loose packing.

TABLE I: Properties of the glass beads used in the experiment.

Particle type	d (mm) ,	$o_s (\mathrm{kg/m^3})$	Size classification
AE	0.12	2530	Very fine particles
В	0.56	2530	Coarse particles

III. NUMERICAL MODEL

The experimental study of the collapse of submerged granular columns can provide results such as collapse process, collapse duration, runout distance and deposit morphology. Pore water motion and the relative motion between the liquid and the solid particles are difficult to measure in the experiment. Solid-liquid two-phase flow simulations, after model verification and validation, can provide information that is difficult to obtain from physical tests and help understand important physics involved in the collapse of submerged granular columns.

The equations governing the conversations of mass and momentum for the solid and liquid phases are summarized here. For a detailed description of the solid-liquid two-phase flow model used in this study, the reader is referred to Lee and Huang ¹⁵.

For the liquid phase, the equation governing the conservation of mass is

$$\frac{\partial \rho_f(1-c)}{\partial t} + \nabla \cdot [\rho_f(1-c)\mathbf{u}^f] = 0, \tag{1}$$

and the equation governing the conservation of momentum is

$$\frac{\partial \rho_f(1-c)\mathbf{u}^f}{\partial t} + \nabla \cdot \left[\rho_f(1-c)\mathbf{u}^f\mathbf{u}^f\right] =
\rho_f(1-c)\mathbf{g} - (1-c)\nabla p_f + \nabla \cdot \left[(1-c)\mathbf{T}^f\right]
- \left\{c\rho_s\frac{\mathbf{u}^f - \mathbf{u}^s}{\tau_p} - \frac{\rho_s}{\tau_p}\frac{(1-c)\nu_{ft}}{\sigma_c}\nabla c\right\}.$$
(2)

For the solid phase, the equation governing the conservation of mass is

$$\frac{\partial \rho_s c}{\partial t} + \nabla \cdot (\rho_s c \mathbf{u}^s) = 0, \tag{3}$$

and the equation governing the conservation of momentum is

$$\frac{\partial \rho_s c \mathbf{u}^s}{\partial t} + \nabla \cdot (\rho_s c \mathbf{u}^s \mathbf{u}^s)
= \rho_s c \mathbf{g} - c \nabla p_f - \nabla (c p_s) + \nabla \cdot (c \mathbf{T}^s)
+ \left\{ c \rho_s \frac{(\mathbf{u}^f - \mathbf{u}^s)}{\tau_p} - \frac{\rho_s}{\tau_p} \frac{(1 - c)\nu_{ft}}{\sigma_c} \nabla c \right\}.$$
(4)

In these equations, ρ_f and ρ_s are the mass densities of the fluid and solid phases, respectively; c is the solid volume fraction (i.e., volumetric concentration); \mathbf{u}^f and \mathbf{u}^s are the mean velocities of the fluid and solid phases, respectively; \mathbf{g} is the gravitational acceleration; p_f is the total pressure of the liquid phase (or pore pressure in this study); p_s is the pressure of the solid phase; \mathbf{T}^f and \mathbf{T}^s are the stress tensors of the liquid and solid phases, respectively; τ_p is the particle response time used to parameterize the inter-phase drag force; ν_{ft} is the eddy viscosity of the liquid phase; and σ_c is the Schmidt number. The two terms in $\{\cdot\}$ in Eqs. (2) and (4) are related to the inter-phase momentum transfer.

The existing solid-liquid two-phase models based on Eqs. (1)-(4) differ from each other in their closure models for \mathbf{T}^f , ν_{ft} , \mathbf{T}^s , p_s , and τ_p . The model of Lee and Huang 15 uses a $k-\epsilon$ model with a low-Reynolds-number correction to compute \mathbf{T}_f and ν_{ft}^{14} , and considers the effects of the turbulent motion of the solid particles in low concentration regions, the elastic effects in high concentration regions, the visco-plastic rheological characteristics and the dilatancy behavior in computing \mathbf{T}^s and p_s . For dense solid-liquid flows, the visco-plastic rheological characteristics and the concentration highly depend on a combined dimensionless parameter, $I = I_v + aI_i^2$, where I_v is the viscous number, I_i is the inertial number, and ais a model parameter¹⁶. The viscous number describes the ratio of the viscous stress to the quasi-static shear stress associated with the weight (resulting from the enduring contact), and is defined by $I_v = 2\rho_f \nu_f D^s/cp_s$, where ν_f = the kinematic viscosity of the fluid, D^s = the second invariant of the strain rate, and d = the particle diameter. The inertial number, defined by $I_i = 2dD^s/\sqrt{cp_s/\rho_s}$, describes the ratio of the inertial stress to the quasi-static stress. Some formulas have been proposed in the literature to describe c-I and $\eta-I$ relationships, where $\eta = T^s/p_s$ with T^s being the second invariant of \mathbf{T}^s . This study adopts the following two formulas for $\eta - I$ and c - I relationships¹⁴:

$$\eta = \eta_1 + \frac{\eta_2 - \eta_1}{1 + I_o/I^{1/2}},\tag{5}$$

where η_2 and I_o are two model parameters and $\eta_1 = \tan \theta_s$ with $\theta_s =$ the angle of repose¹⁶, and

$$c = \frac{c_c}{1 + bI^{1/2}},\tag{6}$$

where c_c is a critical concentration representing the maximum packing fraction of an homogeneously sheared assembly of frictional spheres¹⁷ and b is a model parameter. A brief description of the models for \mathbf{T}^s and p_s can be found in Appendix B. The particle response time, related to the hindered velocity w and volume concentration c, is computed by the following formula¹⁵

$$\tau_p = \frac{\rho_s}{\rho_s - \rho_f} \frac{w}{(1 - c)^2 g},\tag{7}$$

where the hindered velocity w is proportional to the particle fall velocity w_s through a concentration correction proposed by Richardson and Zaki¹⁸, and the fall velocity w_s is computed using the drag formula suggested by White¹⁹.

The key model parameters used in this study are the same as those in Lee and Huang ¹⁵, and summarized in Table II for completeness. Parameters a, b, η_1 , η_2 , and c_c are associated with rheological characteristics, and thus affect the behaviors of the simulated two-phase flows. The value of a was suggested by Lee, Low, and Chiew ¹⁴ based on the experimental results of Bagnold ²⁰. The values of b and c_c were chosen based on the experimental results of Boyer, Pouliquen, and Guazzelli ¹⁷. The values of η_1 and η_2 were suggested experimentally by Cassar, Nicolas, and Pouliquen ² for small glass beads (d = 0.112 mm and 0.21 mm). These parameters are fixed in this study.

TABLE II: Key model parameters used in this study.

The two-phase flow model was developed using OpenFOAM (foam-extend-3.2), which is a free, open-source computational fluid dynamics (CFD) toolbox²¹. The PIMPLE scheme provided by OpenFOAM for the fluid phase is combined with the perditioncorrection scheme²² for the sediment phase¹⁴. This prediction-correction scheme discretizes the mass-balance equation for the sediment phase into an advection-diffusion equation rather than an advection equation. The numerical diffusion behavior can help improve the numerical stability.

Lube et al.²³ experimentally studied in a tank the sub-aerial landslide on a horizontal bed. They measured the spatial distribution of the surface velocity of the spreading granular assembly throughout the sub-aerial landslide process. The measured surface velocity shows that the flow is nearly uniform in the lateral direction during the spreading and commencement phases, except for a very narrow region close to each side wall. At the end of the avalanching phase, the flow almost stops and the granular flow can be regarded as more or less uniform in a narrow region close to the center line of the tank. Therefore, a twodimensional simulation can capture the main features of the collapse process in regions away from the two side walls. Two-dimensional simulations have also been adopted in previous numerical studies of the collapse of granular columns 12,15 . In this study, the two-dimensional computational domain is 0.7 m \times 0.15 m. The grid size used in the simulations ($\Delta x_1 = \Delta x_2$ = 1 mm) was determined based on a grid-dependence test, where two grid sizes were used: $\Delta x_1 = \Delta x_2 = 1$ mm and $\Delta x_1 = \Delta x_2 = 0.5$ mm. Two cases were examined using these two grids. The specifications of these two cases are: d=0.56 mm, $H_i=10$ cm, and $L_i=2$ cm for case 1 and $L_i=5$ cm for case 2. For both cases, the two grid sizes gave nearly identical results: the difference in the computed runout distance was less than 1mm. Therefore, the grid size of $\Delta x_1 = \Delta x_2 = 1$ mm should be fine enough to yield acceptable results.

The value of Courant number must satisfy the following two requirements¹⁴: (1) the value of Courant number in the whole domain must be less than 0.1, and (2) the value of Courant number in high concentration regions (c > 0.55) must be smaller than 0.005.

IV. RESULTS AND DISCUSSIONS

A. Observed and simulated collapse process

Five snapshots of the observed and simulated collapse process for the case of coarse particles (Particle B) with $L_i = 6$ cm and $H_i = 8.9$ cm are shown in Fig. 2, where the instant of time when the gate is fully open is defined as t = 0 s. The reason why we define the origin of time this way is because the release of the gate in the numerical simulation is achieved by instantaneously removing the force that keeps the granular materials in place. The observation is shown in Figs. 2 (a)-(e), and the simulation is shown in Figs.2 (f)-(j). In simulations, the initial concentration affects the deposit topography¹⁵. To obtain a better

agreement with the observation in the simulation, we determined the initial concentration after try-and-error with value between $c_i = 0.55$ and $c_i = 0.55 \times (1 + 0.7\%) = 0.554$. The try-and-error found that $c_i = 0.554$ could give a better agreement with the experiment, which value is fixed in all the simulations. We remark that the initial concentration in the experiment is not vertically uniform in the granular column, with a slightly smaller value near the top and a slightly larger value near the bottom due to the granular weight. The initial collapse process should be controlled mainly by the initial concentration near the failure surface, which difficult to measure in the experiment. The best fitting value of $c_i = 0.554$ in the simulation is believed to reflect the initial concentration near the failure surface to certain extent.

The red solid lines in Figs. 2 (a)-(e) represent the simulated contours corresponding to c = 0.5. Because it is difficult to determine the contour lines for the suspended particles in the experiment, the simulated contours corresponding to $c = 10^{-4}$, 0.01, and 0.5 are included in Figs. 2 (f)-(j) for a qualitatively comparison between the simulation and the observation. It can be seen in Figs. 2 (a)-(e) that in the early stage of the collapse (t < 0.1 s), the top of the column descends with the lower portion of the front face moves forward. From t = 0.1 s to t = 0.8 s the collapse process continues with the granular mass moving forward along the bottom. At t = 1.2 s, the motion of the granular flow virtually stops, but some solid particles are still in suspension at this instant.

Even though the simulated and observed collapse processes agree reasonably well in general, some minor differences can still be observed in the early stages of the collapse process. The minor difference found at t = 0 s to t = 0.4 s are due largely to the difference in the release mechanisms used in the experiment and the simulation: the vertical motion of the gate in the experiment generates an initial vertical current¹⁵, which affects the initial stages of the collapse process. The effect of this initial vertical current in the experiment becomes insignificant in the later stages of the collapse process, say $t \ge 0.8$ s.

The case of very fine particle (Particle AE) has a collapse process similar to that of coarse particle, except that more particles are in suspension for the case of very fine particles, as shown in Fig. 3. For the very fine particles, only the results obtained after the collapse process has stopped are presented and discussed in this study; this is mainly because the large amount of suspended fine particles in the experiment makes it difficult to determine the interface before the moving granular material and the water above.

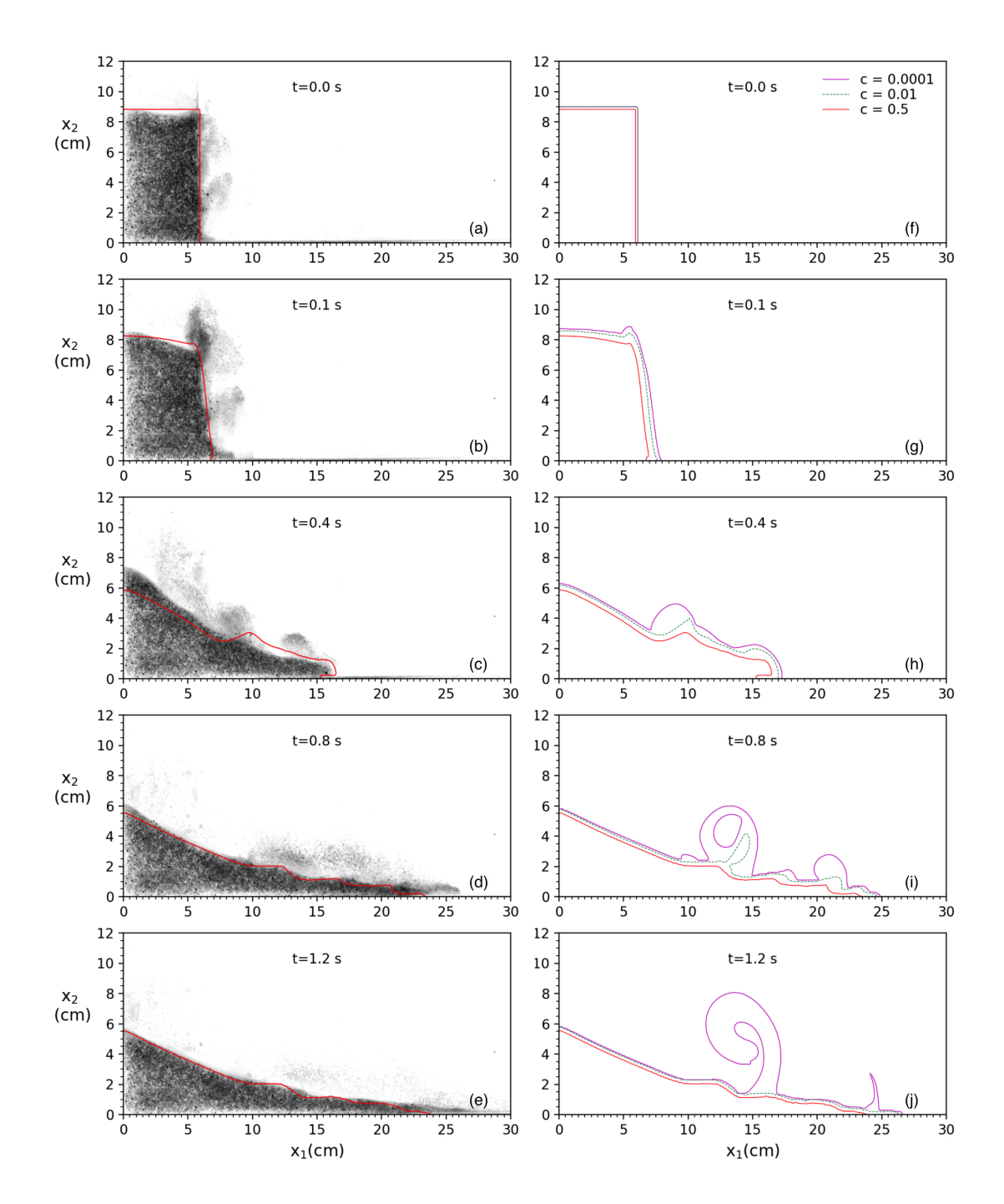


FIG. 2: Comparison of observed [plots (a)-(e)] and simulated [plots(f)-(j)] collapse processes for the coarse particles (Particle B) with $L_i = 6$ cm and $H_i = 8.9$ cm.

B. The simulated velocity and pressure fields of the two phases

The velocity and pressure fields of the two phases are difficult to measure in a physical test, but can be easily provided by a two-phase flow simulation. For the convenience of showing

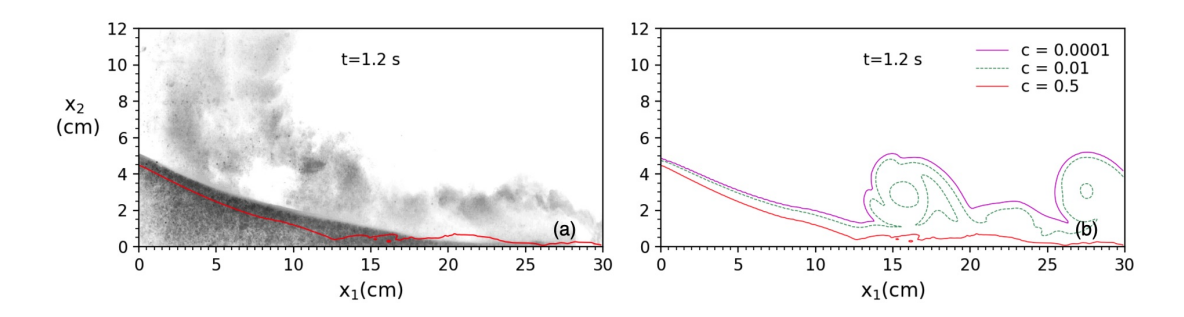


FIG. 3: Comparison of observed (a) and simulated (b) collapse process at t = 1.2 s for the very fine particles (Particle AE) with $L_i = 6$ cm and $H_i = 8.5$ cm.

the pressure variation, only the hydrodynamic part of the fluid pressure, $p_d = p_f - \rho_f g(h - x_2)$, is presented for the fluid phase in the rest of this paper.

Coarse particles

The simulated velocity fields and pressure distributions of the two phases are shown in Fig. 4 for the case of coarse particles (Particle B).

At t = 0.1 s, the right-upper portion of the granular column above the failure surface slides forward down, generating a large vortex in the vicinity of the upper-right corner of the column. The failure angle (θ_f) from the numerical simulation is approximately 52° , which is slightly smaller than θ_f predicted by Mohr-Coulomb failure criterion for dry sand $(\theta_f = 45^{\circ} + \theta_s/2 = 56.2^{\circ})$, where θ_s is the angle of repose²⁴. A zone of positive hydrodynamic pressure exists in the fluid phase in the vicinity of the toe of the column, with the maximum hydrodynamic pressure of a magnitude of 75.1 Pa being found at $x_1 = 6.8$ cm and $x_2 = 0.1$ cm; a zone of negative hydrodynamic pressure accompanies the vortex, which is centered at the upper-right corner of the column. The previous study of Rondon, Pouliquen, and Aussillous by hypothesized that the contractancy occurring at the early stage of the collapse process of a loose-packing column might have contributed to the generation of the positive hydrodynamic pressure inside the column; this hypothesis was later confirmed by the two-phase flow simulation of Lee and Huang ¹⁵. In the present case, the maximum concentration inside the column changes from 0.550 at t = 0 s to 0.556 at t = 0.1 s, an indication of contractancy at the early stage of the collapse process; however, our numerical simulations show that there is no correlation between the location of the maximum hydrodynamic pressure and

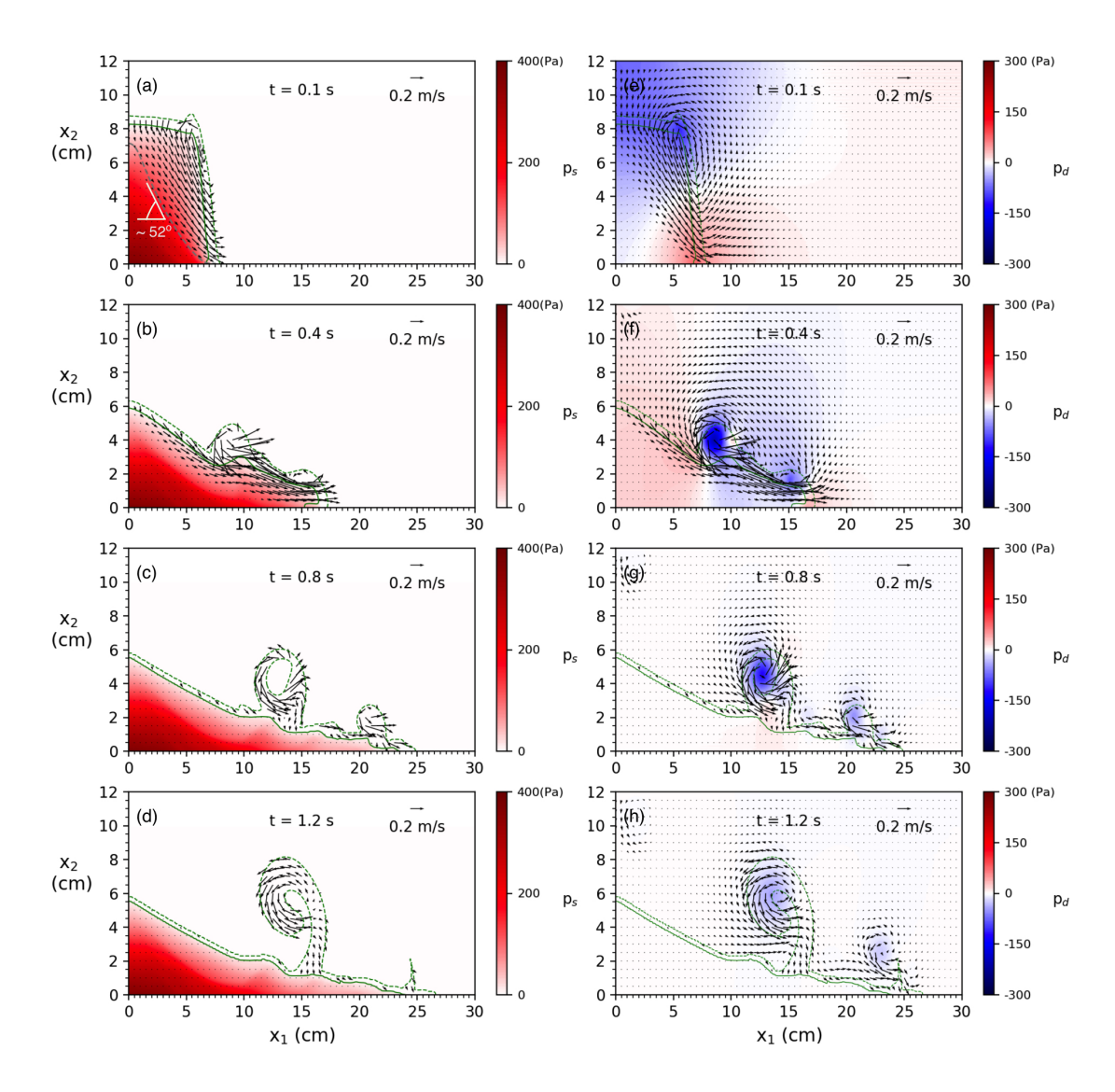


FIG. 4: The simulated flow fields and pressure distributions for the coarse particles (Particle B) with $L_i = 6$ cm and $H_i = 8.9$ cm: the solid phase (a-d) and the fluid phase (e-h). The green solid lines represent contours for the volume concentration c = 0.5 and the green dash lines for c = 0.0001.

the location of the maximum concentration. As for the solid pressure, it increases toward interior of the granular mass in general. We remark that the fluid in the studies of Rondon, Pouliquen, and Aussillous⁵ and Lee and Huang¹⁵ is more viscous than the tap water used in the present study.

At t = 0.4 s, the large vortex formed in the vicinity of the upper-right corner has evolved into at least two vortexes, smaller in size, as the collapse process continues: the one close to the flow front is relatively smaller in size. Each vortex accompanies a zone of negative

hydrodynamic pressure, which penetrates locally into the granular mass. These vortexes cause the solid particles to mix with the fluid, resulting in a near-periodic flow pattern similar to that caused by Kelvin-Helmholtz instability¹⁹. The mixing process and the Kelvin-Helmholtz instability type of flow pattern can also be identified in the snapshots of the observed collapse process shown in Fig. 2 (a)-(e) and in the propagation of other gravity currents²⁵. However, the snapshots of the collapse process of glass beads with d = 3 mm, reported in Meruane, Tamburrino, and Roche⁴, do not show a clear mixing process, possibly because larger particles are difficult to be suspended.

At t = 0.8 s, the two vortexes are in the process of moving away from the granular mass and the zones of negative hydrodynamic pressure accompanying these vortexes completely have moved outside of the granular mass. There is a clear correlation between the pattern of the suspended granular material and the vortex flow pattern. The surface of the granular mass exhibits a wavy shape as a result of the existence of these vortexes.

At t = 1.2 s, the collapse process almost stops because the flow front and the main body of the granular material have stopped moving. However, it takes time for the residual flow associated with these vortexes to disappear and a small amount of suspended particles moving with the residual flow to settle down.

Very fine particles

Fig. 5 shows four snapshots of the simulated flow field and distribution of hydrodynamic pressure for the case of very fine particles (Particle AE). At t = 0.1 s, there exist a zone of negative hydrodynamic pressure and a zone of positive hydrodynamic pressure. Again, the zone of negative hydrodynamic pressure accompanies a large vortex which is centered at the upper-right corner of the column. The zone of positive hydrodynamic pressure occupies the lower portion of the column and extends forward far into the water region in front, with the maximum hydrodynamic pressure of a magnitude of 167.8 Pa being found at x_1 =0 cm and x_2 =0.1 cm. At t=0.4 s, three vortexes can be clearly identified, and each is accompanied by a zone of negative hydrodynamic pressure. At t = 0.8 s, the three vortexes are in the process of moving away from the granular flow with the strength of these vortexes weakened. At t = 1.2 s, the flow front has passed x1= 30 cm, and only one vortex is observable. Note that the negative hydrodynamic pressure does not penetrate into the granular column from

t = 0.4 s onward. Again, the two-phase flow simulation does not show a correlation between the location of the maximum concentration and the location of the maximum pressure.

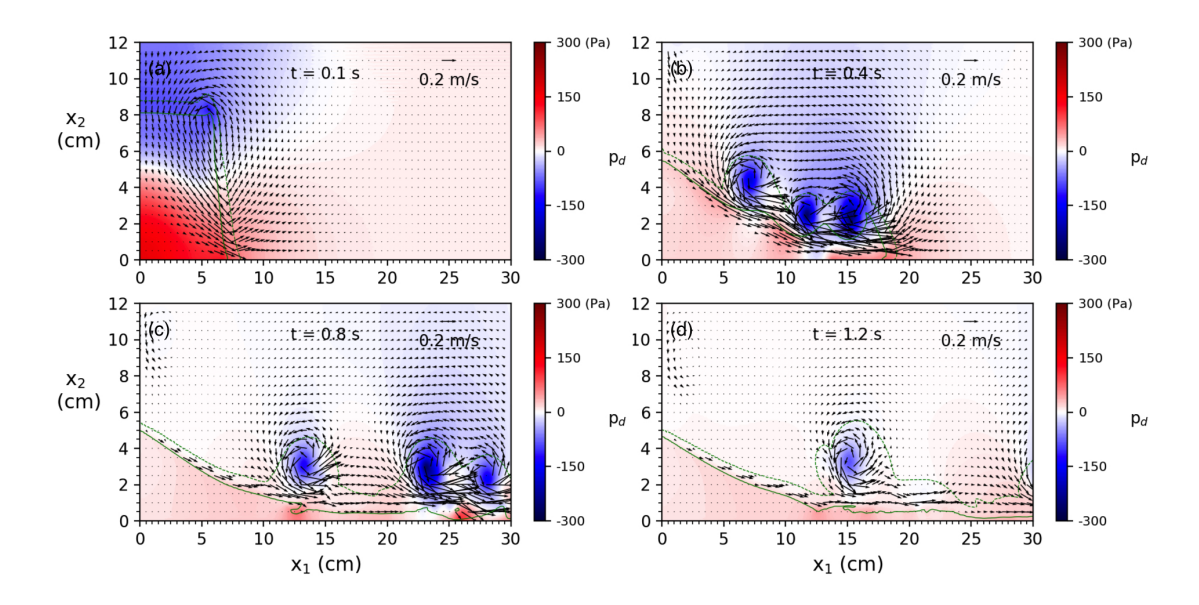


FIG. 5: The computed flow fields and distributions of hydrodynamic pressure of the fluid phase for the very fine particles (Particle AE) with $L_i = 6$ cm and $H_i = 8.9$ cm. The green solid lines represent contours for the volume concentration c = 0.5 and the green dash lines for c = 0.0001.

Discussion on the collapse process and the hydrodynamic pressure

By comparing Figs. 4 and 5, it can be concluded that the positive hydrodynamic pressure at the initial stage of the collapse process for the very fine particles (Particle AE) is much higher than that for the coarse particles (Particle B) and that the collapse duration and the runout distance are longer for the very fine particles under this aspect ratio. The positive hydrodynamic pressure dissipates slower for the very fine particles than in coarse particles due mainly to its low permeability (the permeability of particles is function of grain size squared). The high positive hydrodynamic pressure and its slow dissipation in the very fine particles help increase its fluidity, which in turn increases the collapse duration and runout distance.

Roche *et al.* ²⁶ examined experimentally the time variation of the air pressure on the bed in dry granular flows, and found a pressure drop (i.e., a negative hydrodynamic pressure)

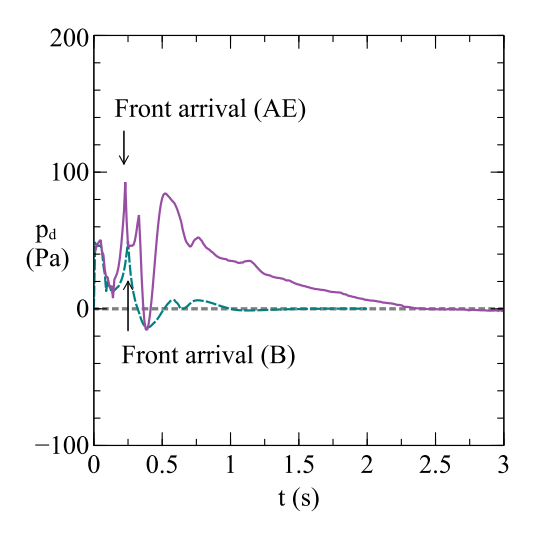


FIG. 6: Variation of computed hydrodynamic pressure at $(x_1, x_2) = (12 \text{ cm}, 0 \text{ cm})$. $L_i = 6 \text{ cm}$ and $H_i = 8.9 \text{ cm}$.

after the passage of the flow front. They hypothesized that this pressure drop might be related to the concentration change (contractancy or dilatancy). The time series of the simulated hydrodynamic pressure on the bed at $x_1 = 12$ cm and $x_2 = 0$ cm are presented in Fig. 6. After the arrival of the flow front, the hydrodynamic pressure is negative first and then positive for both cases, which is consistent with the finding of Roche et al. ²⁶, and the hydrodynamic pressure on the bed gradually disappears as the collapse process approaches its final stage. The simulated flow fields shown in Figs. 4 and 5 reveal that the strong fluctuation of the pressure at a point on the bed is closely related to the negative pressure zones accompanying with the vortexes. However, for the very fine particles (Particle AE), a positive hydrodynamic pressure can be built up because of the low permeability and the low pressure dissipation rate associated with it.

C. Relative motion between the two phases

The drag force acting on the solid phase by the liquid phase is $c\rho_s(\mathbf{u}^f - \mathbf{u}^s)/\tau_p$ with τ_p being the particle response time. Therefore, the relative velocity $\mathbf{u}^f - \mathbf{u}^s$ can be used to represent the magnitude and direction of the drag force acting on the solid phase by the liquid phase. Fig. 7 shows four snapshots of the simulated relative velocity for the coarse particles (Particle B) with $L_i = 6$ cm and $H_i = 8.9$ cm (see Fig. 2 for the corresponding velocity fields). At t = 0.1 s, the passive motion of the fluid phase is caused by the motion

of the solid phase along the failure surface, which is driven by the gravitational force. At t=0.4 s, the gravitational force has less effect on the forward motion of the solid phase near the flow front; as a result, the forward motion of the solid phase near the flow front is driven mainly by the drag force imposed by the fluid phase on the solid phase through the vortexes accompanying the granular flow (see Fig. 2 (f)); therefore, a greater influence of the vortexes on the granular flow is expected in the later stages of the collapse process. At the final stage of the collapse process, the drag force gradually diminishes and the the motion of the granular mass eventually stops.

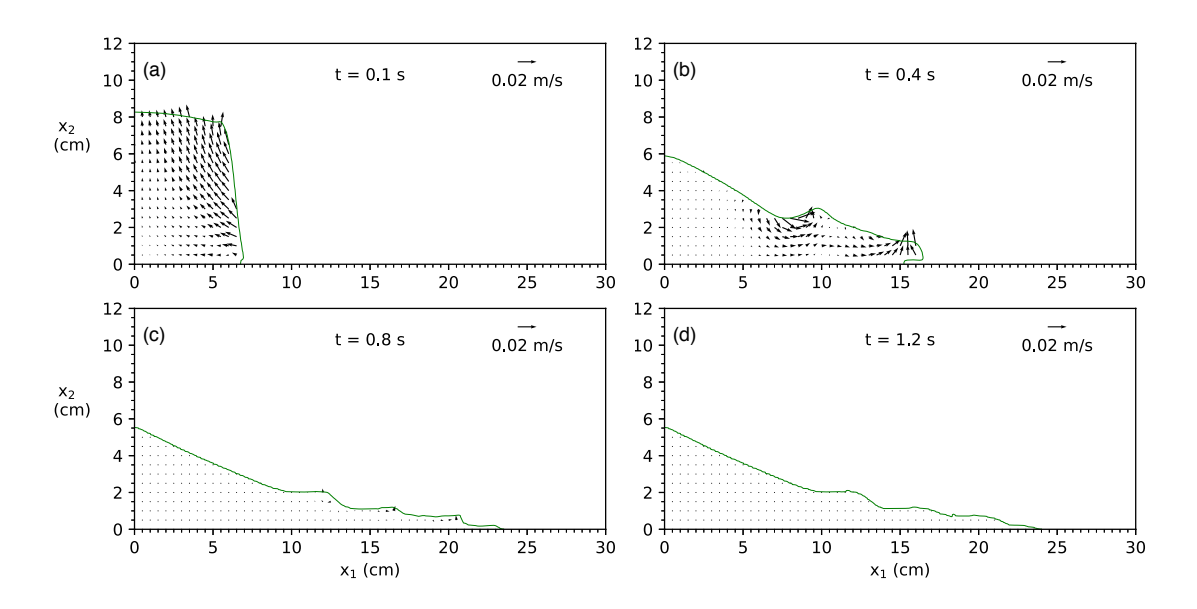


FIG. 7: Snapshots of the relative velocity $\mathbf{u}^f - \mathbf{u}^s$ for the coarse particles (Particle B).

D. Effects of initial aspect ratio and particle size

Similar to dry granular columns^{6,27}, the initial aspect ratio of a granular column is a key parameter affecting the collapse process and deposit morphology of the submerged granular column⁵. Because particle size can affect the rheology of a submerged granular flow¹⁶, it may also affect the collapse process of the submerged granular column, which, however, is less understood. This section examines, through the two-phase flow simulations supported by the laboratory results, possible effects of the aspect ratio and particle size on the collapse process, deposit morphology, spread velocity, collapse duration, final height and runout distance.

Modes of collapse process and types of deposit morphology

The initial collapse of a granular column submerged in water is driven by the gravitational force, which causes the granular material above the failure surface to move. Our numerical results show that the initial collapse of the granular column is related to the so-called toe failure, which is characterized by the failure surface passing through the toe and extending backward up. Toe failure is typical for steep slopes of homogeneous granular material. Our numerical simulations also show two modes of the initial collapse process and three types of final deposit morphology, depending on the initial aspect ratio $A = H_i/L_i$: (i) if the initial aspect ratio is large (say $A > A_L$) so that the initial failure surface is deeply buried down in the column, then the entire upper portion of the column descends at the initial stage of the collapse process, causing the granular material in the lower portion of the column to slide forward down along a smaller failure surface (referred to as "descending collapse mode" in this study); (ii) if the initial aspect ratio is small (say $A < A_L$) so that the failure surface is not buried deep enough in the column, then a significant portion of the top layer slides forward down along the larger failure surface at the initial stage of the collapse process (referred to as "sliding collapse mode" in this study). Our numerical results show that this critical value of A, denoted by A_L , is about 3 for both coarse and very fine particles. Four examples are shown in Fig. (8), where Fig. 8 (a) and (b) are for $A > A_L$, and Fig. 8 (c) and (d) are for $A < A_L$.

For $A > A_L$, the final deposit morphology can have either a "Mexican hat" shape (an almost flat outer region with a depressed, steep central region)^{27,28} or a triangular shape, depending on another critical value of A, denoted by A_M . If $A > A_M$ (i.e., the length of the column is critically small compared to its height), the failure surface is so small that there is not enough shear force from the failure surface to resist the motion of the granular material; as a result, the entire column descends like a free fall and when the top layer of the granular mass hits the bottom it pushes out the granular material at the base of the column (similar to a high-speed water jet impacting a surface), creating a final deposit morphology like a "Mexican hat" (see Fig. 8 (a)). However, if $A < A_M$, the shear force from the failure surface can provide some resistance to the descending of the granular material so that the descending velocity of the column is smaller than that for $A > A_M$; therefore, the downward momentum is not large enough to make the top layer to have a direct impact

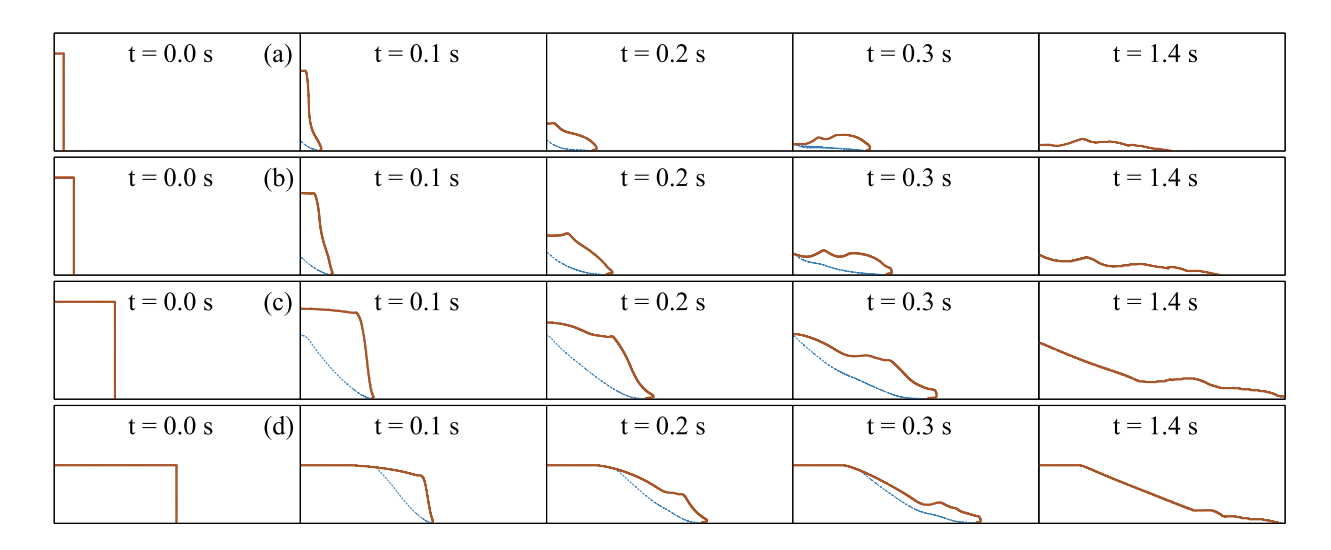


FIG. 8: Collapses of submerged granular columns for the coarse particles (Particle B) with (a) A = 10 ($L_i = 1$ cm and $H_i = 10$ cm), (b) A = 5 ($L_i = 2$ cm and $H_i = 10$ cm), (c) A = 1.67 ($L_i = 6$ cm and $H_i = 10$ cm), and (d) A = 0.5 ($L_i = 12$ cm and $H_i = 6$ cm). The red solid lines are the contour lines of c = 0.5. The blue dotted lines are the failure surface defined by $|\mathbf{u}_1| = 5$ cm/s. The final deposit morphology is a "Mexican hat" for (a), a triangular shape (b and c), or a trapezoid shape (d).

with the bottom, and the final deposit morphology has a triangular shape (see Fig. 8 (b)). Our numerical results give $A_M = 8.0$ for both the coarse and very fine particles. We remark that the exact value of A_M for dry granular columns was not given in Lagrée, Staron, and Popinet²⁷; however, from the results presented in Lagrée, Staron, and Popinet²⁷, the value of A_M for dry granular columns should be smaller than 67.9.

For $A < A_L$, the final deposit shape depends on a third critical value of A, denoted by A_H . If $A > A_H$, the failure surface does not intersect during the entire collapse process; as a result, final deposit morphology has a triangular shape (see Fig. 8 (c)); if $A < A_H$, the column is wide enough so that the failure surface intersects with the top surface of the column during the entire collapse process; as a result, a portion of the top layer is never affected by the collapse process, and the final deposit morphology has a trapezoidal shape (see Fig. 8 (d)). Our numerical results give $A_H = 0.75$ for the coarse particles (B particles) and $A_H = 0.6$ for the very fine particles (AE particles). We also determined A_H from our experimental results: $A_H = 0.87$ for Particle B and $A_H = 0.53$ for Particle AE. The measured values of A_H are close to the simulated ones ($A_H = 0.75$ for Particle B and $A_H = 0.6$ for

Particle AE).

For the collapse of a dry granular column, the dynamics of the granular flow and the final deposit morphology also depend three critical values of the initial aspect ratio²⁷: $A_L \approx 3.0$, $A_H \approx 0.7$, and $3.0 < A_M < 67.0$.

It is remarked here that for the collapse of a granular column submerged in a high viscous fluid, Rondon, Pouliquen, and Aussillous⁵ also observed that the final deposit morphology could be either triangular-shaped or trapezoid-shaped, depending on the initial packing c_i and the critical aspect ratio A_H which varied in the range of 0.1 to 0.7 for $c_i \approx 0.54 - 0.57$.

We also remark that, in our experiment, the initial aspect ratio is in the range of A = 0.2 and 4, which makes it impossible to determine A_M from our experiment results because $A_M \approx 8$ according to our simulation results. Additionally, our upper limit of A in the experiment is too close to A_L ($A_L \approx 3$ from the simulations), which makes it inappropriate to determine A_L using the experimental results.

Spreading velocity and collapse duration

The moving flow front is difficult to determine from the video recording due to the strong mixing in the vicinity of the flow front and the resulting highly-diffusive interface between the granular mass and the water (see Fig. 3). This is especially true for very fine particles. Therefore, only the results obtained when the collapse process has stopped are presented hereinafter. The spreading velocity (the velocity of the flow front) and the collapse duration presented are determined from the two-phase flow simulations using the concentration contour corresponding to a specified concentration, say c = 0.5.

To define the spreading velocity and the collapse duration, an example of the simulated time series of the flow-front location x_f (extracted from the concentration contour line for c = 0.5) is shown in Fig. 9 for the coarse particles (Particle B) with $L_i = 6$ cm and $H_i = 8.9$ cm. Three stages of the flow-front motion can be identified: (I) an acceleration stage (t < 0.2 s), (II) a nearly-constant velocity (0.2s < t < 0.5s), (III) a deceleration stage (t > 0.5s). The velocity at stage (II) is defined as the spreading velocity, denoted by u_f . These three stages have also been identified in the studies of dry granular columns⁶. We remark that Meruane, Tamburrino, and Roche⁴ has also observed that the spreading velocity is nearly constant between the acceleration and deceleration stages for submerged granular columns.

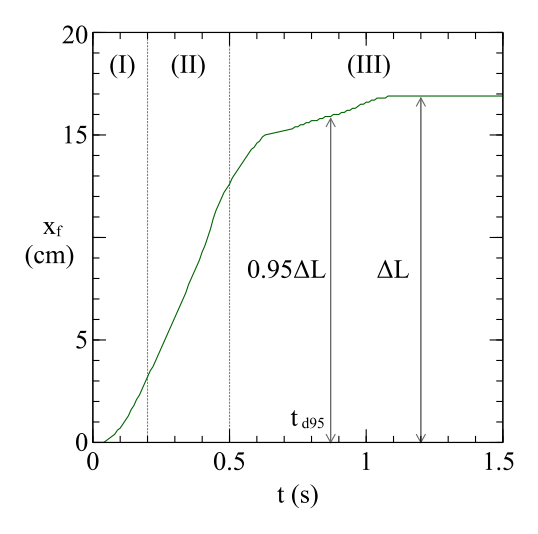


FIG. 9: An example of the simulated location of the flow front x_f for the coarse particles (Particle B) with $L_i = 6$ cm and $H_i = 8.9$ cm. ΔL is the runout distance and t_{d95} is the collapse duration.

The collapse duration is also determined from the time series of the flow-front location x_f . For some cases, the vortexes moving with the flow front can cause strong mixing locally, and the particles entrained in the vortexes may influence the determination of the flow-front location at the final stage of the collapse process. Therefore, we follow Rondon, Pouliquen, and Aussillous⁵ and represent the collapse duration by t_{d95} , which is the time it takes for the sliding material to travel a distance equal to 95% of the runout distance ΔL , as shown in Fig. 9.

Fig. 10 shows the normalized spreading velocity, $u_f/\sqrt{g'L_i}$, as a function of the initial aspect ratio A for both the coarse particles (Particle B) and the very fine particles (Particle AE). Similar to the collapse of dry granular columns⁴, $u_f/\sqrt{g'L_i}$ increases with increasing A. The following empirical relation can be obtained from the two-phase flow simulation results:

$$\frac{u_f}{\sqrt{g'L_i}} \propto \begin{cases} A^{1/2}, & A < A_L \\ A^{1/3}, & A > A_L \end{cases}$$
(8)

where $A_L \approx 3$, which has been mentioned in Section IV D where we discussed the collapse process and the deposit morphology. When $A < A_L$, the length of the column is long enough so that the initial length of the column is no longer a factor affecting the spreading velocity. However, when $A > A_L$, the upper portion of the column descends, pushing the lower portion of the column forward; as a result, u_f depends on both H_i and L_i .

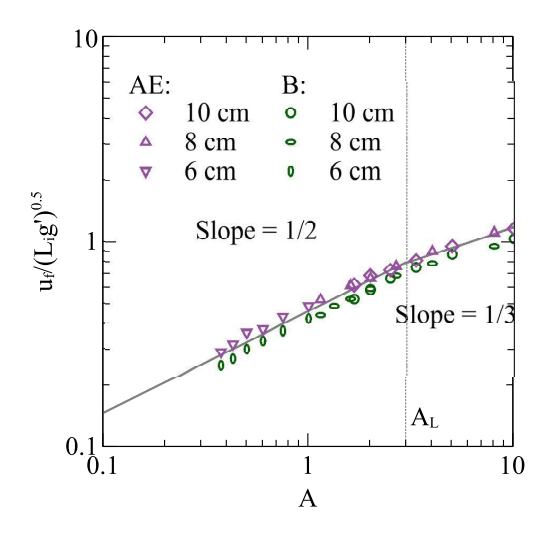


FIG. 10: Effect of the initial aspect ratio (A) on the normalized spreading velocity $(u_f/\sqrt{L_i g'})$. The numbers in the legend are the values of H_i . Data are from the simulations.

Our numerical results also show that finer particles spread faster. The effect of particle size on the spreading velocity is possibly related to the positive hydrodynamic pressure in the granular material: the small permeability in the very fine particles helps build up a larger positive hydrodynamic pressure (Fig. 6), which in turn reduces the solid-phase pressure²⁴ and friction.

We remark that the observation of Meruane, Tamburrino, and Roche⁴ on the spreading velocity is different from ours. Their results show that coarser particles give a larger spreading velocity. Because the initial concentration can significantly affect the collapse process⁵, we believe the difference in the initial concentration may have contributed to this discrepancy: the initial concentration is $c_i \approx 0.6$ in Meruane, Tamburrino, and Roche⁴, but $c_i \approx 0.55$ in the present study.

Fig. 11 shows the simulated change of normalized collapse duration, $t_{d95}/\sqrt{L_i/g'}$, with initial aspect ratio A. The following empirical relation can be obtained from the two-phase flow simulation results:

$$\frac{t_{d95}}{\sqrt{L_i/g'}} \propto \begin{cases} A^{1/2}, \ A < A_H \\ A^{1/3}, \ A > A_H \end{cases} \tag{9}$$

Our numerical results suggest the collapse duration $t_{d95} \propto g'^{-1/2} H_i^{1/3} L_i^{1/6}$ for $A > A_H$. Based on their DEM simulation results for the collapse of submerged granular columns,

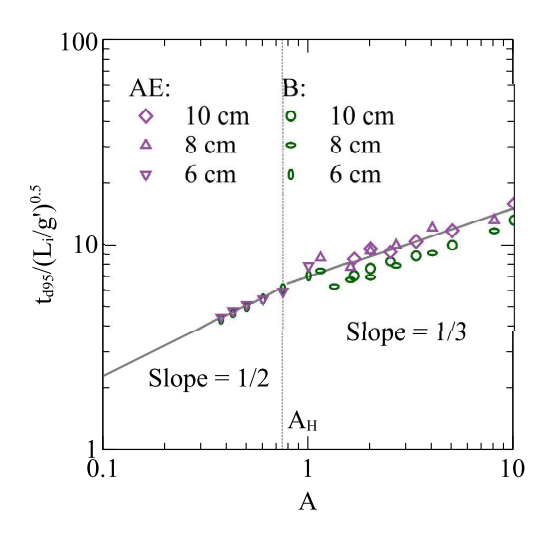


FIG. 11: The simulated change of normalized collapse duration with initial aspect ratio A.

The numbers in the legend are the values of H_i .

Topin et al.⁸ also found that t_{d95} depended on both H_i and L_i . The collapse duration $t_{d95} \propto \sqrt{H_i/g'}$ for $A < A_H$ (i.e., if the column is long enough, the length of the column will not be a factor affecting the collapse duration), which is similar to that for dry granular columns where t_{d95} depends only on H_i^6 .

It is interesting to note that the collapse duration for the very fine particles (Particle AE) is the same as that for the coarse particles (Particle B) if $A < A_H$, i.e. the final deposit morphology is trapezoidal. However, the very fine particles have a longer collapse duration than the coarse particles if $A > A_H$.

Final height and runout distance

The measured and simulated changes of dimensionless final height (the maximum height of the final deposit), H_f/L_i , with initial aspect ratio A are shown in Fig. 12. For comparison, the simulation results of Lee, Huang, and Chiew²² for dry granular columns are also included in Fig. 12 (a) and the experimental results of Rondon, Pouliquen, and Aussillous⁵ for granular columns submerged in a high viscous fluid are superposed in Fig. 12 (b). In general, the simulation agrees with the measurement well and our experimental results are consistent with the previous experimental ones⁵. The following empirical relationship can

be obtained from the measured and simulated final heights:

$$\frac{H_f}{L_i} \propto \begin{cases} A, & A \lesssim A_H \\ A^{1/3}, & A_H \lesssim A \lesssim A_L \end{cases}$$
 (10)

When $A \lesssim A_H$, H_f/L_i increases linearly with A, suggesting $H_f = H_i$ and a trapezoid-

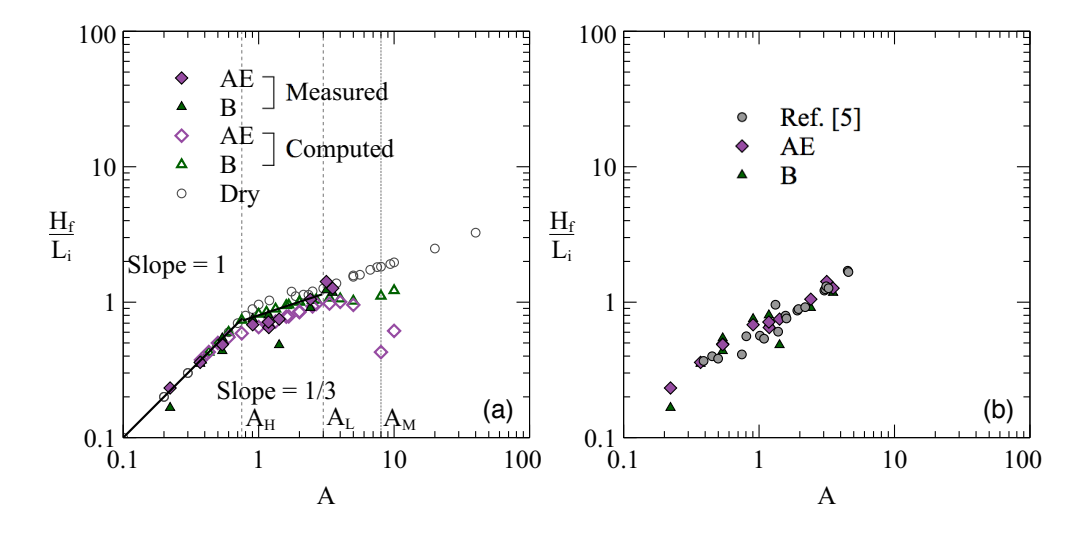


FIG. 12: Normalized final heights of granular columns against the aspect ratio. (a)
Comparison with dry granular column¹⁴. (b) Comparison with experimental results of Rondon, Pouliquen, and Aussillous⁵.

shaped deposit morphology. The value of A_H depends on particle size: $A_H = 0.6$ for the very fine particles (Particle AE) and $A_H = 0.75$ for the coarse particles (Particle B). When $A_H \lesssim A \lesssim A_L$ ($A_L \approx 3.0$), H_f/L_i increases with $A^{1/3}$. When $A \gtrsim A_L$, the dependence of H_f/L_i on the aspect ratio A is not clear. As mentioned in Section IV D, the collapse process for $A \gtrsim A_L$ differs from those for $A \lesssim A_L$. The particle size does not seem to have a significant effect on the value of H_f/L_i when $A < A_L$. As shown in Fig. 12, H_f/L_i for dry columns is larger than those for submerged columns, which is consistent with the conclusions of Rondon, Pouliquen, and Aussillous⁵ for initially loosely-packed submerged granular columns in a high viscous fluid. When $A \gtrsim A_M$ ($A_M \approx 8$), the values of H_f/L_i for the very fine particles (Particle AE) drop suddenly due to the large vertical momentum during the collapse process (referring to the discussion on Figs. 8 (a) and (b)). Additionally, the values of H_f/L_i for the very fine particles (Particle AE) are much smaller than those for the coarse particles (Particle B). There exist studies investigating A_H , A_L , and A_M for

dry granular columns (e.g. Roche $et~al.^{26}$), which have been discussed in Lee, Huang, and Chiew 22 .

An intuitive explanation is provided here: when $A \gtrsim A_M$ the top portion of the column descends like a free fall and the final deposit topography has a "Mexican hat" shape (as we discussed in Section IV D); in the process of creating the "Mexican hat" morphology, the very fine particles (Particle AE) can be pushed farther away from the base of the column due to its high fluidity and easiness for suspension, resulting in a smaller final height.

The measured and simulated changes of dimensionless runout distance, $\Delta L/L_i = (L_f - L_i)/L_i$, with the aspect ratio A are shown in Fig. 13. For comparison, the simulation results of Lee, Huang, and Chiew²² for dry granular columns are included in Fig. 13 (a) and the measured results of Rondon, Pouliquen, and Aussillous⁵ for submerged granular columns in loose-packing condition in Fig. 13 (b). Referring to Fig. 13 (b), our experimental results agree with the previous results well⁵.

The following empirical relationship can be obtained from the measurement and simulation results:

$$\frac{\Delta L}{L_i} \propto \begin{cases} A, & A \lesssim A_L \\ A^{2/3}, & A \gtrsim A_L \end{cases} \tag{11}$$

Meruane, Tamburrino, and Roche⁴ studied the collapse of submerged granular columns

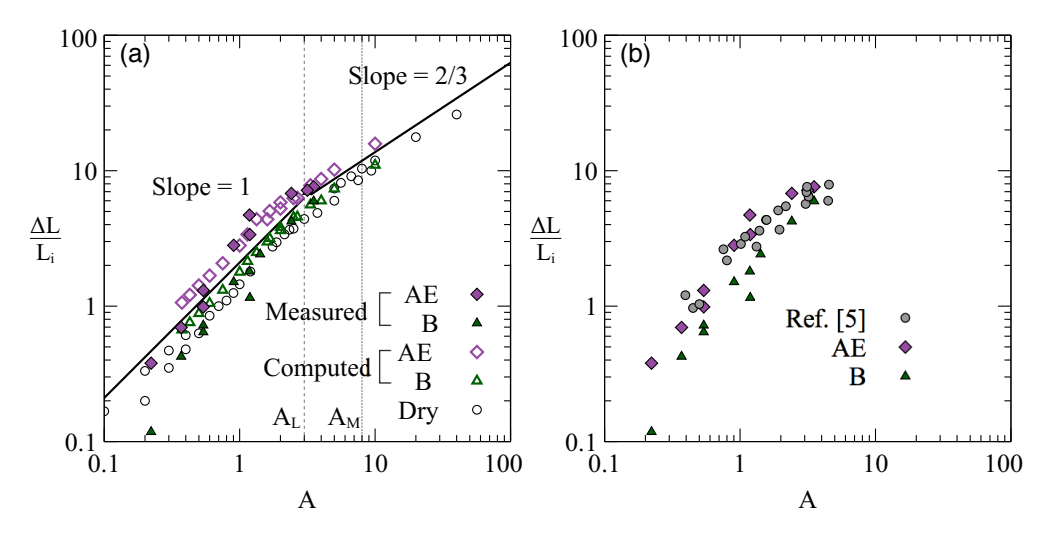


FIG. 13: Changes of the normalized runout distance with the initial aspect ratio A. (a) Comparison with dry granular column²². (b) Comparison with experimental results of Rondon, Pouliquen, and Aussillous⁵.

with initially-dense packing condition and suggested that $\Delta L/L_i \propto A$ for $A \lesssim A_L$ and

 $\Delta L/L_i \propto A^{0.56}$ for $A \gtrsim A_L$. It is believed that the difference in the exponents in the expressions for $\Delta L/L_i$ for $A > A_L$ is due to the different initial concentrations used in the present study and the study of Meruane, Tamburrino, and Roche 4 ($c_i \approx 0.55$ in the present study but $c_i \approx 0.6$ in the study of Meruane, Tamburrino, and Roche⁴; the effect of initial concentration c_i on the scaling law has been discussed by Rondon, Pouliquen, and Aussillous⁵). It can be observed in Fig. 13 (a) that the granular column with a smaller particle size produces a longer runout distance because a granular column with smaller particles has a faster propagation speed and a longer propagation duration, as shown in Section IV D. Compared to the dry granular columns, the submerged granular columns have a similar dependence of $\Delta L/L_i$ on A, but the submerged columns have longer runouts in general. This is consistent with the conclusions of Topin et al.⁸, who hypothesized that during the collapse process of the column, the presence of fluid could reduce the kinetic energy of solid phase and enhance the flow of the granular material through lubrication. Our two-phase flow simulation results suggest that in the later stages of the collapse process, the effects of gravity is weak and it is the horizontal momentum associated with the vortexes in the fluid phase that moves the solid phase forward through the drag force between the two phases (see Fig. 7); however, the air flow cannot provide enough drag force in the case of dry columns because of the small density of the air.

V. CONCLUSIONS

The collapse of a submerged granular column in loose packing was studied experimentally and numerically. The numerical simulations were performed using a two-phase flow model, which was verified and validated using a set of experimental results. Very fine particles (d=0.12 mm) and coarse particles (d=0.56 mm) were considered in order to examine the effects of particle size. For each particle size, the collapse of the granular column was examined for a range of initial aspect ratios. The following conclusions can be drawn based on a combination of the experimental and numerical results.

1. Under the initial aspect ratio, A, the spreading velocity and runout distance for the very fine particles were found to be larger than those for coarse particles. The collapse duration for the very fine particles is the same as that for the coarse particles when the final deposit morphology is trapezoidal.

- 2. Two types of initial collapse processes were identified. The critical aspect ratio, A_L , that separates these two types of collapse processes was about 3.0 for both particle sizes. When the aspect ratio is larger than A_L , the failure surface is deeply buried down in the column and the entire top layer descends at the initial stage of the collapse process; when the aspect ratio is smaller than A_L , the failure surface is not deep enough so that a significant portion of the top layer moves along the failure surface.
- 3. Two other critical aspect ratios that determine the final deposit morphology were determined based on the numerical results: (i) $A_M \approx 8.0$, and (ii) $A_H \approx 0.6$ for the very fine particles and $A_H \approx 0.75$ for the coarse particles. When $A < A_H$, the final deposit morphology has trapezoidal shape; when $A > A_M$ the final deposit morphology has a "Mexican hat" sape; otherwise, the final deposit morphology has a triangular shape.
- 4. During the collapse process, several vortexes were observed in both the experiment and the numerical simulation, and their formation might be related to the so-called Kelvin-Helmholtz instability. The presence of these vortexes were found to be responsible for the pressure drop on the bed immediately after the passage of the flow front and the wavy feature on the final deposit morphology. The numerical simulation also revealed that the motion of the flow front in the later stages of the collapse process were strongly affected by these vortexes, which is, however, not the case for dry granular columns because of the low density of the air.
- 5. From the numerical simulation results, it was found that the variations of the runout distance, final deposit height, collapse duration, and spreading velocity were piece-wise functions of the initial aspect ratio.

Appendix A: Determination of initial concentration

There are two methods to determine the initial fraction of loosely-packed glass beads used in the experiment, both of which are based on measuring the volume of a given amount of glass beads with known weight.

The first method follows the following procedure:

1. A two-liter beaker is partially filled with water.

- 2. Glass beads with known mass m are poured into the beaker; the volume of all glass beads is known by $V_b = m/\rho_s$, where ρ_s is the density of the beads provided by manufacture.
- 3. The mixture of water and glass beads is stirred and then allow the suspended glass beads to completely settle down.
- 4. The bulk volume of the loosely-packed glass beads V is determined by measuring the location of the interface between the water and the packed glass beads,
- 5. The initial fraction is $c_i = V_b/V$.

The second method is to use the same procedure in-situ. However, the loss of glass beads through the gaps between the gate and the side walls may cause errors in the measured bulk volume, which is especially a concern for fine particles. The first method is recommended because we believe the first method can give more accurate measurement of the initial fraction.

In our experiment, the first method was adopted and the amount of glass beads used to measure the initial fraction was 2kg, and repeating tests showed that the measured mean initial fraction was 0.55 with a relative error of $\pm 0.7\%$.

Appendix B: Stress and pressure of the solid phase

Using a regularization technique that regards the static sediment as a very viscous fluid²⁹, \mathbf{T}^s is expressed as

$$\mathbf{T}^{s} = -\left(\frac{2}{3}\rho_{s}\nu_{s}\nabla\cdot\mathbf{u}^{s}\right)\mathbf{I} + 2\rho_{s}\nu_{s}\mathbf{D}^{s},\tag{B1}$$

where \mathbf{D}^s is the strain rate and ν_s is the kinematic viscosity for the sediment phase. Here, ν_s is modeled by

$$\nu_s = \nu_{sv} + \nu_{st},\tag{B2}$$

where ν_{sv} and ν_{st} account for the rheological characteristics (visco-plastic effect) and turbulence effects, respectively. The pressure of the sediment phase is a superposition of three components

$$p_s = p_{sr} + p_{se} + p_{st},\tag{B3}$$

where p_{sr} reflects the rheological characteristics when the sediment is in motion, p_{se} accounts for the elastic effect when sediment is in its static state, and p_{st} accounts for the turbulent motion of sediment phase. Here, only the two components ν_{sv} and p_{sr} are presented due to

their relations to rheological characteristics of high concentration flows. The former (ν_{sv}) is computed by

$$\nu_{sv} = \frac{(p_{sr} + p_{se})\eta}{2\rho_s D^s},\tag{B4}$$

where η is given by Eq. (5). The later (p_{sr}) is determined by

$$p_{sr} = \frac{2b^2c}{(c_c - c)^2} (\rho_f \nu_f + 2a\rho_s d^2 D^s) D^s$$
 (B5)

according to Eq. (6).

ACKNOWLEDGMENTS

This study is supported partially by the Ministry of Science and Technology, Taiwan (MOST 106-2221-E-032 -029) and the U.S. National Science Foundation under the grant No. CBET 1706938. Any opinions, findings, and conclusions or recommendations expressed in this material are those of the author(s) and do not necessarily reflect the views of the National Science Foundation. This is SOEST contribution No.10571.

REFERENCES

- ¹C. T. Crowe, "On models for turbulence modulation in fluidparticle flows," Int. J. Multiph. Flow **26**, 719–727 (2000).
- ²C. Cassar, M. Nicolas, and O. Pouliquen, "Submarine granular flows down inclined planes," Phys. Fluids **17**, 103301 (2005).
- ³E. L. Thompson and H. E. Huppert, "Granular column collapses: Further experimental results," J. Fluid Mech. **575**, 177–186 (2007).
- ⁴C. Meruane, a. Tamburrino, and O. Roche, "On the role of the ambient fluid on gravitational granular flow dynamics," J. Fluid Mech. **648**, 381 (2010).
- ⁵L. Rondon, O. Pouliquen, and P. Aussillous, "Granular collapse in a fluid: role of the initial volume fraction," Phys. Fluids **23**, 73301 (2011).
- ⁶E. Lajeunesse, J. B. Monnier, and G. M. Homsy, "Granular slumping on a horizontal surface," Phys. Fluids **17**, 103302 (2005).
- ⁷G. Lube, H. E. Huppert, R. S. J. Sparks, and A. Freundt, "Static and flowing regions in granular collapses down channels," Phys. Fluids 19, 43301 (2007).

- ⁸V. Topin, Y. Monerie, F. Perales, F. Radjaï, and F. Radjaï, "Collapse dynamics and runout of dense granular materials in a fluid," Phys. Rev. Lett. **109**, 188001 (2012).
- ⁹C. Wang, Y. Wang, C. Peng, and X. Meng, "Dilatancy and compaction effects on the submerged granular column collapse," Phys. Fluids **29**, 103307 (2017).
- ¹⁰A. C. Santomaso, S. Volpato, and F. Gabrieli, "Collapse and runout of granular columns in pendular state," Phys. Fluids 30, 063301 (2018).
- ¹¹S. B. Savage, M. H. Babaei, and T. Dabros, "Modeling gravitational collapse of rectangular granular piles in air and water," Mech. Res. Commun. **56**, 1–10 (2014).
- ¹²P. Si, H. Shi, and X. Yu, "Development of a mathematical model for submarine granular flows," Phys. Fluids **30**, 083302 (2018).
- ¹³C. Meruane, a. Tamburrino, and O. Roche, "Dynamics of dense granular flows of small-and-large-grain mixtures in an ambient fluid," Phys. Rev. E 86, 026311 (2012).
- ¹⁴C.-H. Lee, Y. M. Low, and Y.-M. Chiew, "Multi-dimensional rheology-based two-phase model for sediment transport and applications to sheet flow and pipeline scour," Phys. Fluids 28, 053305 (2016).
- ¹⁵C.-H. Lee and Z. Huang, "A two-phase flow model for submarine granular flows: With an application to collapse of deeply-submerged granular columns," Adv. Water Resour. 115, 285–300 (2018).
- ¹⁶M. Trulsson, B. Andreotti, and P. Claudin, "Transition from the Viscous to Inertial Regime in Dense Suspensions," Phys. Rev. Lett. 109, 118305 (2012).
- ¹⁷F. Boyer, O. Pouliquen, and E. Guazzelli, "Dense suspensions in rotating-rod flows: normal stresses and particle migration," J. Fluid Mech. **686**, 5–25 (2011).
- ¹⁸J. Richardson and W. Zaki, "Sedimentation and fluidisation: Part I," Chem. Eng. Res. Des. 32, S82–S100 (1954).
- $^{19}\mathrm{F.}$ White, $\mathit{Viscous}$ fluid flow (McGraw-Hill, Singapore, 2000).
- ²⁰R. A. Bagnold, "Experiments on a Gravity-Free Dispersion of Large Solid Spheres in a Newtonian Fluid under Shear," Proc. R. Soc. London, Ser. A 225, 49–63 (1954).
- ²¹H. Jasak, "OpenFOAM: Open source CFD in research and industry," Inter. J. Nav. Arch. Oc. Engng. **1**, 89–94 (2009).
- ²²C.-H. Lee, Z. Huang, and Y. M. Chiew, "A three-dimensional continuum model incorporating static and kinetic effects for granular flows with applications to collapse of a two-dimensional granular column," Phys. Fluids **27**, 113303 (2015).

- ²³G. Lube, H. E. Huppert, R. S. J. Sparks, and A. Freundt, "Collapses of two-dimensional granular columns," Phys. Rev. E **72**, 41301 (2005).
- ²⁴B. M. Das, *Principles of Geotechnical Engineering* (PWS Publishing Company, Boston, 2013).
- ²⁵A. Dai, "Experiments on gravity currents propagating on different bottom slopes," J. Fluid Mech. **731**, 117–141 (2013).
- ²⁶O. Roche, M. Attali, A. Mangeney, and A. Lucas, "On the run-out distance of geophysical gravitational flows: Insight from fluidized granular collapse experiments," Earth Planet. Sci. Lett. 311, 375–385 (2011).
- 27 P.-Y. Lagrée, L. Staron, and S. Popinet, "The granular column collapse as a continuum: validity of a two-dimensional NavierStokes model with a μ (i)-rheology," J. Fluid Mech. 686, 378–408 (2011).
- ²⁸E. Lajeunesse, A. Mangeney-Castelnau, and J. P. Vilotte, "Spreading of a granular mass on a horizontal plane," Phys. Fluids **16**, 2371–2381 (2004).
- ²⁹J. Chauchat and M. Médale, "A three-dimensional numerical model for dense granular flows based on the $\mu(I)$ rheology," J. Comput. Phys. **256**, 696–712 (2014).